SLAC-PUB-16104

First characterization of coherent optical vortices from harmonic undulator radiation

E. Hemsing, M. Dunning, C. Hast, and T. Raubenheimer

SLAC National Accelerator Laboratory,

Menlo Park, California 94025, USA

Dao Xiang

Key Laboratory for Laser Plasmas (Ministry of Education),

Department of Physics and Astronomy,

Shanghai Jiao Tong University, Shanghai 200240, China

Abstract

We describe the experimental generation and measurement of coherent light that carries orbital angular momentum from a relativistic electron beam radiating at the second harmonic of a helical undulator. The measured helical phase of the light is shown to be in agreement with predictions of the sign and magnitude of the phase singularity, and is more than two orders of magnitude greater than the incoherent signal. Our setup demonstrates that such optical vortices can be produced in modern free electron lasers in a simple afterburner arrangement for novel two-mode pump-probe experiments.

Submitted to Physical Review Letters.

This work was supported at SLAC by the US Department of Energy under contract DE-AC02-76SF00515 and BES.

Modern free-electron lasers (FELs) generate coherent light down to hard x-rays and femtosecond pulse durations for fundamental research on the behavior of matter [1, 2]. The output light is transversely coherent with a Gaussian-like transverse profile and is polarized according to the orientation of the magnets in the FEL undulator. To meet the growing diversity of demands for users, new and more sophisticated techniques have emerged recently to enhance the control over the output light, enabling two color operations [3–7], pump-probe experiments [8], and fast polarization switching up to 1 kHz rates [9–12]. These schemes typically require minor modifications to the FEL layout, such as tuning the undulators to different resonant wavelengths or the addition of a dispersive section and second undulator immediately downstream of the FEL. The latter 'afterburner' setup produces optical and x-ray pulses synchronized to within a few femtoseconds for pump-probe experiments [13], or can be used to control the polarization of the output light in fast polarization-switching schemes where the undulator is orthogonally polarized.

Here, we experimentally examine a proof-of-principle technique using this simple afterburner configuration for another class of experiments that require laser pulses that carry orbital angular momentum (OAM). In contrast to previous more complicated schemes [14], this arrangement specifically exploits the angular emission characteristics of helical undulators to generate OAM light. Combined with multi-color, pump-probe, or polarization switching schemes, this technique may be used to exploit the additional degrees of freedom provided by OAM light to broaden the scientific scope of modern FELs, including those operating at longer wavelengths.

In 1992, Allen et al [15] noted that cylindrically symmetric solutions to the paraxial wave equation in the form of Laguerre-Gaussian (LG) modes carry a helical phase and $l\hbar$ units of OAM per photon where l is an integer. Since then, LG beams and their more general *optical vortex* counterparts have become the subject of intense study for increasingly diverse research applications such as imaging, quantum entanglement, optical pumping, and microscopy (see e.g., Refs. [16–18] and references therein). For example, in stimulated emission-depletion fluorescence microscopy (STED), the null on-axis intensity profiles of OAM beams can be used to beat the diffraction limit [19–21]. Akin to pump-probe experiments, STED uses two successive laser pulses with different transverse profiles to first excite then quench molecules everywhere except for within a highly localized probe volume. The OAM carried by the electromagnetic (EM) field can also be precisely exchanged with atoms, molecules, and

macroscopic materials. At x-ray wavelengths, OAM light has been suggested for expanded x-ray magnetic circular dichroism to distinguish spin-polarized atomic transitions through angle-resolved energy loss spectrometry [22].

Optical vortices are typically generated by passing the laser beam through a mask or other dedicated mode-conversion optics (see, e.g, [23–25]). While such techniques can be extended to x-rays [26], e-beams in FEL undulators provide an alternate and non-invasive vortex production method that is widely tunable and not restricted by the EM field intensity [27, 28]. This enables the production of intense OAM light over the full range of wavelengths accessible to FELs. In general, the wavelength of the light emitted by a beam with energy $E = \gamma mc^2$ in an undulator is

$$\lambda = \frac{\lambda_u}{2h\gamma^2}\left(1 + K^2 + \gamma^2\theta^2\right), \tag{1}$$

where λ_u is the undulator period, K is the rms undulator field strength, and θ is the radiation opening angle. Light at harmonics h is also emitted, and has an off-axis annular intensity profile for all $h > 1$ in helical undulators [29]. In Ref. [30] it was predicted that the accompanying phase structure of the harmonic radiation also carries an azimuthal component that is characteristic of OAM light. This has since been confirmed in recent experiments on second harmonic incoherent undulator radiation (IUR) from a 3rd generation synchrotron light source [31]. These measurements utilized a pinhole scan technique that revealed the helical structure of the IUR through the transverse interference pattern generated from light emitted in successive undulator sections.

For IUR, the distribution of the OAM light is determined only by the angular spectral emission characteristics of the undulator, provided that the beam emittance is not large compared to the diffraction limited source size of the undulator radiation [31]. In this case, enhanced control over the OAM light can be obtained with coherent undulator radiation (CUR), for which the complex EM field distribution also depends on the 3D e-beam distribution. A typical method to produce CUR is illustrated in Fig. 1, where the e-beam is first modulated in energy through its interaction with a laser in an undulator. A dispersive chicane then converts the modulation into a density modulation, which then emits CUR in the subsequent undulator. There are two ways in which CUR that carries OAM can be

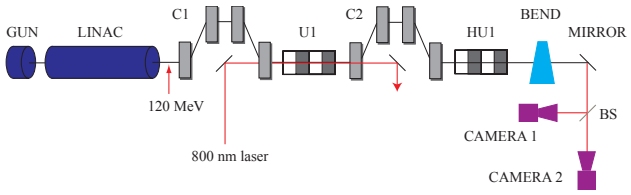

FIG. 1: Schematic of the harmonic OAM experiment at SLAC-NLCTA. The 120 MeV beam is modulated by the 800 nm laser in the U1 planar undulator, and radiates OAM light at harmonics of the HU1 helical undulator that is captured by two cameras.

produced in this setup. They are both governed by the general relation [32],

$$l_b = l \pm (h-1), \tag{2}$$

which describes the coupling between OAM light of the form $e^{ikz-il\phi}$ at harmonic undulator frequencies and screw-type modulations in the e-beam distribution described by a $e^{ikz-il_b\phi}$ dependence. The + or - sign indicates the right or left handedness of the helical undulator field.

In one method, a simple Gaussian laser ($l = 0$) tuned to a harmonic resonance of a helical undulator generates a helical modulation in the e-beam that then radiates OAM light. This was observed indirectly in [33], and directly in [14]. In the latter setup, a Gaussian ($l = 0$) IR laser at 800 nm was used to modulate the energy of a 120MeV e-beam inside a right-handed helical undulator tuned such that 800 nm was resonant with the $h = 2$ undulator resonance. From Eq. (2), this produced an e-beam with a $l_b = 1$ helical modulation that then radiated a coherent $l = 1$ optical vortex at the fundamental frequency in a downstream planar undulator.

Here we experimentally examine the second method, in which coherent OAM is generated according to Eq. (2) in a reversed setup. Namely, the e-beam is modulated in the conventional sense without a helical dependence ($l_b = 0$) inside a planar undulator, and then radiates a coherent optical vortex at the harmonics of a downstream helical undulator. This models an FEL afterburner-type arrangement, in which the $l_b = 0$ modulation is generated by the standard FEL lasing process. Accordingly, compared to the first method in [14], this method has two distinct advantages. First, the layout is simpler in that a chicane and helical undulator can be added to the end of an existing FEL to generate coherent OAM from the structure already on the beam. Second, it does not require that a helical bunching structure

in the e-beam be generated and preserved during transport. In this experiment, we find that radiation at the second harmonic of the helical undulator produces an $l = -1$ vortex, in agreement with Eq. (2) and interestingly, opposite in helicity to the case from [14] where the planar and helical undulator positions are switched. In this sense, the arrangement is similar to a previous experiment that confirmed the hollow transverse intensity profile of harmonic CUR [34], but did not examine the transverse phase to confirm the presence of optical vortices.

A layout of the experiment, carried out at the Next Linear Collider Test Accelerator (NLCTA) at SLAC [35–37] is shown in Fig. 1. The electron beam with ∼5 pC charge is generated in a 1.6 cell S-band (2.856 GHz rf frequency) photocathode gun with a UV laser (1 ps FWHM) and further accelerated to 120 MeV with X-band (11.424 GHz) linac structures. The beam is positioned at the gun phase so that it leaves with the minimum energy spread and has a measured rms length of $\simeq$ 300 fs. A 1 ps FWHM Ti:Sapphire laser pulse at 800 nm is sent into the first undulator U1 (10 periods of 3.3 cm each and normalized rms magnetic field strength K=1.28) where it interacts with the electron beam to imprint a sinusoidal energy modulation. Chicane C1 produces an orbit bump to allow on-axis interaction between the e-beam and laser in U1. Chicane C2 is set to $R_{56} = 2$ mm to turn the induced energy modulation into a periodic density modulation, which generates coherent bunching at 800 nm. The beam then radiates light in the helical undulator HU1 (4 periods, λ_u=5.26 cm, K=1.52) which is tuned to a fundamental of 1600 nm. Thus, the bunching generated at 800 nm radiates coherently at the second harmonic of HU1.

Radiation from HU1 is reflected off an in-vacuum extraction mirror 60 cm downstream and sent through a beam splitter to two CCD cameras that can capture images simultaneously. Camera 1 (focal length of 48 cm) images the plane of the in-vacuum mirror 34 cm away. This also serves as a beam positioning setup via the optical transition radiation (TR) emitted when the e-beam strikes the mirror. Camera 2 (focal length of 10.8 cm) captures the far-field with the focus set to infinity. This combination of different image planes enables iterative reconstruction of the transverse phase of the radiation profile from the measured intensities for each shot.

Just downstream of the undulator is a variable magnetic dipole which allows one to deflect the e-beam vertically on the screen. Because the radiation from HU1 is unaffected, this is used to control the direction of the TR emitted from the dump mirror into the diagnostic

cameras.

With the e-beam fully deflected by the dipole to remove the TR signal, the far field radiation from the undulator was recorded with Camera 2 (Fig. 2). While no filters were used, the response of the optical setup is optimized to collect light specifically around 800 nm. With the modulating laser off, only the incoherent undulator radiation (IUR) is observed. A line-out across the center of the IUR donut is shown as the blue line in Fig. 2. The angular width of the off-axis peaks is found to be θ=4.3 mrad. With the laser on, the coherent harmonic emission from the bunched beam has a peak intensity that is 400 times larger than the IUR (red line, Fig. 2). The angular distribution is also significantly narrowed, indicating that the transverse e-beam size contributes to the angular emission profile. In this sense, we obtain control over the OAM light distribution in that it can be tailored by the e-beam size and focused to a tighter spot than IUR. The measured θ=1 mrad angular spread is consistent with the measured 120 μm rms e-beam size in the undulator. With the 800±5 nm band pass filter inserted the coherent signal is seen to be essentially unaffected, which shows that the observed coherent signal is dominated by the second harmonic. The filtered incoherent signal was observed to have a narrower angular spread (not shown), peaking at θ=1.6 mrad, as expected from analysis.

With the modulating laser on, the coherent TR (CTR) signal can be used to explicitly reveal the OAM phase structure of the second harmonic CUR through interference, similar to the technique exploited in Ref [31]. With the deflecting magnet turned off, the bunched beam radiates both in the undulator and at the ejection mirror. The CUR from HU1 interferes coaxially with the CTR from the mirror downstream, producing a spiral-like intensity variation in the far-field profile at Camera 2. Experimental results from our setup are shown

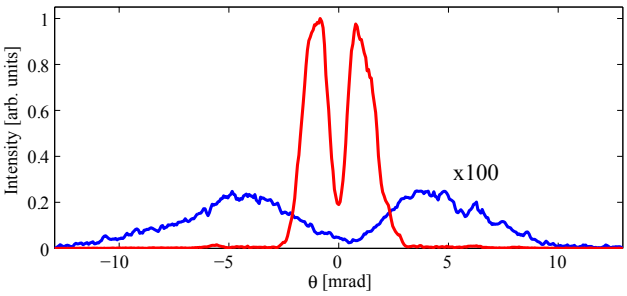

FIG. 2: Comparison between incoherent (blue) and coherent (red) undulator radiation profiles. The wider incoherent signal is multiplied by a factor of 100.

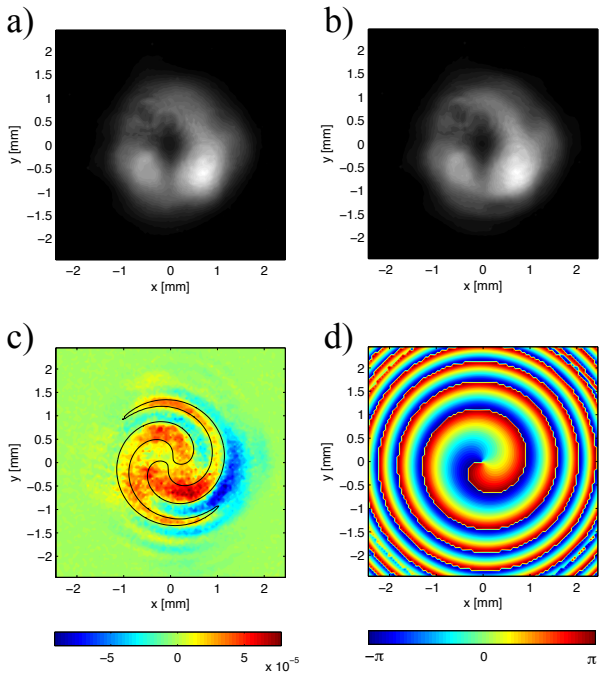

FIG. 3: a) Measured far field CUR from the second harmonic. b) Measured far field profiles of CUR and CTR emitted coaxially, from different longitudinal positions. c) The difference between images a and b. d) Predicted CUR phase carrying $l = -1$ structure.

in Fig 3. In the upper left image, Fig. 3a, the far field profile of only the second harmonic CUR at 800 nm is shown, where the deflecting magnet is turned on strongly to completely remove the CTR. In Fig 3b, the profile is shown with the deflecting magnet turned off. Though subtle, an interference pattern is observable from the combination of CUR and CTR in the far field. The interference is revealed by subtracting Fig 3b from Fig 3a in post-processing. The difference, shown in Fig. 3c, is a clear swirling intensity pattern that reveals the $l = -1$ OAM in the CUR. The structure can be understood by examination of the different features of the CUR and CTR. The CUR is circularly polarized light with an $l = -1$ helical phase. The weaker but still visible CTR from the screen is radially polarized, but carries no helical phase because it is generated by the e-beam with simple $l_b = 0$ bunching. The theoretically predicted structure shows a two-armed spiral pattern that is shown as an overlay contour in Fig. 3c, and closely matches the experimental result. The theoretical pattern was calculated using the well-known analytic expressions for CUR and CTR emitted from the measured longitudinal positions 1.04 m and 0.44 m away from the camera, respectively. The calculated phase from the CUR used to generate the overlay interference pattern is shown in Fig. 3d. The striking similarity between the observed interference pattern and the predicted pattern

support the presence of the $l = -1$ coherent OAM light emitted at the second undulator harmonic.

Further evidence of the OAM structure is obtained visually when the e-beam is only slightly deflected by the bend magnet. In this case, shown in Fig. 4, the undisturbed CUR interferes with off-axis CTR emitted by the vertically deflected beam. Off-axis CTR light has a somewhat simpler structure in the sense that it interferes with the CUR in a manner that is similar to a tilted plane wave with linear polarization. The observed far field profile in Fig. 4a shows distinct evidence of the interplay between the CUR and CTR in the apparent intensity striping. Subtracting this image from the CUR-only profile in Fig. 3a again reveals the signature edge dislocation "fork" pattern of interference generated near the central phase singularity (Fig. 4b, black arrow) of an $l = -1$ vortex [25].

Finally, the intensity profiles from the CUR from both cameras was processed with an iterative phase retrieval algorithm to extract the transverse phase structure. The procedure is similar to standard techniques and uses Huygens transport integrals back and forth between the two image planes to reconstruct the phase from the measured intensities and known optics [38]. Starting from random phase noise (ie., a random phase value between $[-\pi, \pi]$ for each pixel), the algorithm proceeds until it converges to a specified value or stagnates, as measured by the difference between the measured amplitudes and reconstructed amplitudes each iteration cycle. The routine consistently arrives at the results shown in Fig. 5, which indicate a dominant $l = -1$ structure. The measured intensity from Camera 1 is shown in Fig. 5a, and the extracted phase in Fig. 5b. Similarly, the far field intensity from Camera 2 is shown in Fig. 5c, and its phase in Fig. 5d. We note the similarity between the reconstructed phases and the theoretically predicted phase from second harmonic CUR shown in Fig. 3d.

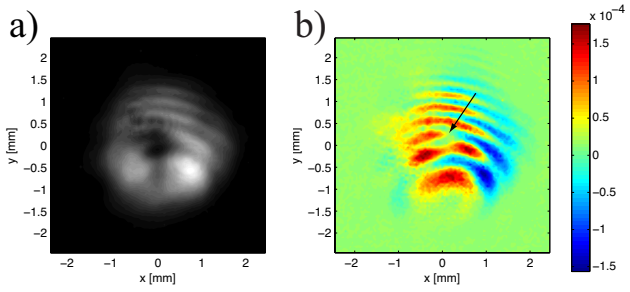

FIG. 4: Interference between CUR and off-axis CTR reveals the signature forked pattern of a $l = -1$ vortex from the second harmonic undulator emission.

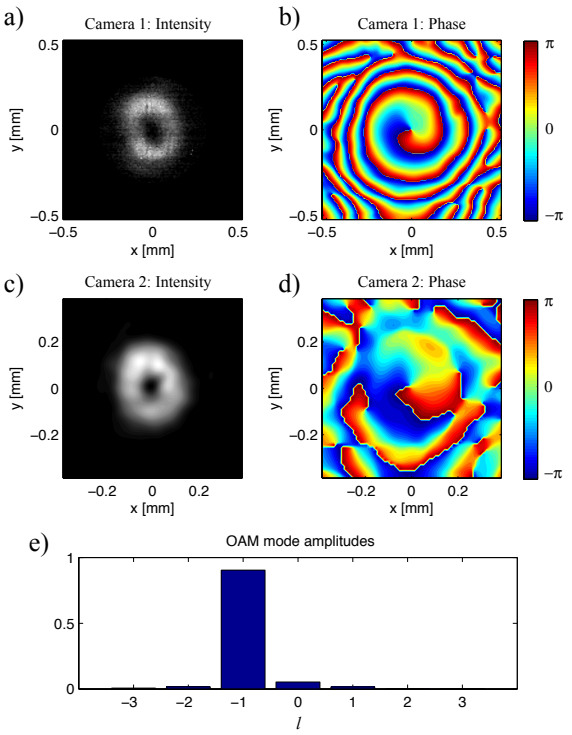

FIG. 5: Measured intensity (a) and reconstructed phase (b) of CUR emission from camera 1. Measured intensity (c) and reconstructed phase (d) of CUR emission from camera 2 from the same shot. Bottom: l-mode amplitudes from mode decomposition of reconstructed fields.

Shown at the bottom in Fig. 5e is the distribution of OAM l-modes contained in the beam [14]. This is calculated by a mode decomposition on the reconstructed complex field, and shows that over 91% of the power is contained in the $l = -1$ mode.

Together with the results presented in [14], results of this experiment indicate that the predicted relationship $l_b = l \pm (h-1)$ between the coherent bunching structure in the e-beam and the helical phase from the undulator holds true for 2nd harmonic interactions. The novel afterburner arrangement investigated here however, is simpler and more broadly usable for practical applications. Given its simplicity, such a setup could be straightforwardly implemented in x-ray FELs to generate intense coherent OAM light for novel research by placing a properly tuned helical undulator downstream of the FEL. By this technique, density bunching generated through the standard lasing process at the fundamental upstream could then radiate at a harmonic of the helical undulator. For practical designs with $N_p \gg 1$ periods, the number of photons at the second harmonic frequency can be expected to be approximately $K^2/2N_p(1+K^2)$ times fewer than at the fundamental. The total FEL output would be two x-ray pulses that carry different values of OAM for new types of pump-probe ex-

periments. Such an arrangement could also be used in polarization switching schemes with pairs of helical undulators that would allow the polarization to be varied while the l-mode number remains fixed. Alternately, the helical undulator could be tuned to emit harmonics in the optical regime as an FEL afterburner that also carries OAM.

We thank the NLCTA facility staff for their assistance, and A. Knyazik for building the helical undulator. This work was supported both by the U.S. DOE Office of Basic Energy Sciences using the NLCTA facility which is partly supported by U.S. DOE Office of High Energy Physics under Contract No. DE-AC02-76SF00515 and the National Natural Science Foundation of China under Grant No. 11327902.

[1] P. Emma et al., Nat Photon **4**, 641 (2010).

[2] T. Ishikawa, H. Aoyagi, T. Asaka, Y. Asano, N. Azumi, T. Bizen, H. Ego, K. Fukami, T. Fukui, Y. Furukawa, et al., Nat Photon **6**, 540 (2012).

[3] A. A. Lutman, R. Coffee, Y. Ding, Z. Huang, J. Krzywinski, T. Maxwell, M. Messerschmidt, and H.-D. Nuhn, Phys. Rev. Lett. **110**, 134801 (2013).

[4] A. Marinelli, A. A. Lutman, J. Wu, Y. Ding, J. Krzywinski, H.-D. Nuhn, Y. Feng, R. N. Coffee, and C. Pellegrini, Phys. Rev. Lett. **111**, 134801 (2013).

[5] F. Ciocci, G. Dattoli, S. Pagnutti, A. Petralia, E. Sabia, P. L. Ottaviani, M. Ferrario, F. Villa, and V. Petrillo, Phys. Rev. Lett. **111**, 264801 (2013).

[6] M. Labat, N. Joly, S. Bielawski, C. Szwaj, C. Bruni, and M. E. Couprie, Phys. Rev. Lett. **103**, 264801 (2009), URL `http://link.aps.org/doi/10.1103/PhysRevLett.103.264801`.

[7] G. De Ninno, B. Mahieu, E. Allaria, L. Giannessi, and S. Spampinati, Phys. Rev. Lett. **110**, 064801 (2013), URL `http://link.aps.org/doi/10.1103/PhysRevLett.110.064801`.

[8] E. Allaria, F. Bencivenga, R. Borghes, F. Capotondi, D. Castronovo, P. Charalambous, P. Cinquegrana, M. B. Danailov, G. de Ninno, A. Demidovich, et al., Nature Communications **4**, 2476 (2013).

[9] K.-J. Kim, Nuclear Instruments and Methods in Physics Research Section A: Accelerators, Spectrometers, Detectors and Associated Equipment **445**, 329 (2000), ISSN 0168-9002.

[10] C. Snchez-Hanke, C.-C. Kao, and S. Hulbert, Nuclear Instruments and Methods in Physics Research Section A: Accelerators, Spectrometers, Detectors and Associated Equipment **608**,

351 (2009), ISSN 0168-9002.

[11] Y. Ding and Z. Huang, Phys. Rev. ST Accel. Beams **11**, 030702 (2008).

[12] H. Deng, T. Zhang, L. Feng, C. Feng, B. Liu, X. Wang, T. Lan, G. Wang, W. Zhang, X. Liu, et al., Phys. Rev. ST Accel. Beams **17**, 020704 (2014).

[13] E. L. Saldin, E. A. Schneidmiller, and M. V. Yurkov, Phys. Rev. ST Accel. Beams **13**, 030701 (2010).

[14] E. Hemsing, A. Knyazik, M. Dunning, D. Xiang, A. Marinelli, C. Hast, and J. B. Rosenzweig, Nature Phys. **9**, 549 (2013).

[15] L. Allen, M. W. Beijersbergen, R. J. C. Spreeuw, and J. P. Woerdman, Phys. Rev. A **45**, 8185 (1992).

[16] G. Spalding, J. Courtial, and R. D. Leonard, *Structured Light and Its Applications: An Introduction to Phase-Structured Beams and Nanoscale Optical Forces* (Academic Press, 2008), 1st ed., ISBN 0123740274.

[17] L. Allen, S. M. Barnett, and M. J. Padgett, *Optical angular momentum* (Institute of Physics Pub., 2003), ISBN 0750309016.

[18] G. Molina-Terriza, J. P. Torres, and L. Torner, Nat Phys **3**, 305 (2007).

[19] S. W. Hell and J. Wichmann, Opt. Lett. **19**, 780 (1994).

[20] S. W. Hell, Nature Biotechnology pp. 1347–1355 (2003).

[21] P. Török and P. Munro, Opt. Express **12**, 3605 (2004).

[22] B. T. Thole, P. Carra, F. Sette, and G. van der Laan, Phys. Rev. Lett. **68**, 1943 (1992).

[23] M. W. Beijersbergen, L. Allen, H. E. L. O. Van der Veen, and J. P. Woerdman, Optics Communications **96**, 123 (1993).

[24] M. W. Beijersbergen, R. P. C. Coerwinkel, M. Kristensen, and J. P. Woerdman, Optics Communications **112**, 321 (1994).

[25] N. R. Heckenberg, R. McDuff, C. P. Smith, H. Rubinsztein-Dunlop, and M. J. Wegener, Optical and Quantum Electronics **24**, S951 (1992).

[26] A. G. Peele, P. J. McMahon, D. Paterson, C. Q. Tran, A. P. Mancuso, K. A. Nugent, J. P. Hayes, E. Harvey, B. Lai, and I. McNulty, Opt. Lett. **27**, 1752 (2002).

[27] E. Hemsing and A. Marinelli, Phys. Rev. Lett. **109**, 224801 (2012).

[28] P. c. v. R. Ribič, D. Gauthier, and G. De Ninno, Phys. Rev. Lett. **112**, 203602 (2014).

[29] W. Colson, IEEE J. Quant. Elect. **17**, 1417 (Aug 1981).

[30] S. Sasaki and I. McNulty, Phys. Rev. Lett. **100**, 124801 (2008).

[31] J. Bahrdt, K. Holldack, P. Kuske, R. Müller, M. Scheer, and P. Schmid, Phys. Rev. Lett. **111**, 034801 (2013).

[32] E. Hemsing, P. Musumeci, S. Reiche, R. Tikhoplav, A. Marinelli, J. B. Rosenzweig, and A. Gover, Physical Review Letters **102**, 174801 (2009).

[33] E. Hemsing, A. Knyazik, F. O'Shea, A. Marinelli, P. Musumeci, O. Williams, S. Tochitsky, and J. B. Rosenzweig, Applied Physics Letters **100**, 091110 (pages 4) (2012).

[34] E. Allaria, F. Curbis, M. Coreno, M. Danailov, B. Diviacco, C. Spezzani, M. Trovó, and G. DeNinno, Phys. Rev. Lett. **100**, 174801 (2008).

[35] D. Xiang, E. Colby, M. Dunning, S. Gilevich, C. Hast, K. Jobe, D. McCormick, J. Nelson, T. O. Raubenheimer, K. Soong, et al., Phys. Rev. Lett. **105**, 114801 (2010).

[36] D. Xiang, E. Colby, M. Dunning, S. Gilevich, C. Hast, K. Jobe, D. McCormick, J. Nelson, T. O. Raubenheimer, K. Soong, et al., Phys. Rev. Lett. **108**, 024802 (2012).

[37] E. Hemsing, D. Xiang, M. Dunning, S. Weathersby, C. Hast, and T. Raubenheimer, Phys. Rev. ST Accel. Beams **17**, 010703 (2014).

[38] L. Allen and M. Oxley, Optics Communications **199**, 65 (2001).